Available online www.ejaet.com

European Journal of Advances in Engineering and Technology, 2023, 10(1):15-31

Research Article ISSN: 2394 - 658X

A Novel Architecture Pid/Lqrt-Pso Trajectory Tracking Based on Dual Duty Cycle Modulation Driver for 2wd Mobile Robots

Markov Mbihi Djoumessi*, Bertrand Moffo Lonla and Leandre Nneme Nneme

Laboratory of Computer Science Engineering and Automation, University of Douala,
P.O.Box 1872 Douala, Cameroon
*Corresponding author: mbihimarkov@yahoo.fr

ABSTRACT

This research paper presents a relevant contribution to a novel architecture of 2WD mobile robot including dual drivers and kinematic controller for stabilizing tracking trajectory. The two drivers based on Pulse Width Modulation (PWM) and Duty Cycle Modulation (DCM) are modeled in Matlab/Simulink and applied directly on dynamic servomechanism in open Loop and also applied in closed Loop through PID/LQRT-PSO control. Kinematic controller based on inverse kinematic model is designed in order to guarantee system stability using Lyapunov function. Simulation obtained in the same operating conditions for optimal trajectory tracking are presented and discussed in this paper. An analysis of these results shows using Dual DCM drivers in the trajectories tracking loop of a 2WD mobile robot, is a challenge compared to classic Dual PWM drivers. In fact, Dual DCM drivers brings lower hardware complexity, less intricate switching effects, and better transient and steady performance of the overall optimal feedback control system.

Key words: 2WD mobile robot, kinematic controller, PWM driver, Dual DCM driver, PID/LQRT-PSO control, Lyapunov function

---

1. INTRODUCTION

The modern duty cycle modulation (DCM) technique initiated since 2005 in [1], has been a foundation for the design and implementation of new devices in electronic systems engineering.

Among the main application domains already well conquered by DCM are A/D conversion [2]–[5], D/A conversion [6], signal transmission via a wired or optical channel [7], signal transmission systems[8], control drivers for DC-DC [9]–[11] and DC-AC power electronic converters [12],[13]. This abundant literature, which demonstrates the immense transversality of DCM technical services, has motivated us to consider extending the scope of DCM impact to robotic control systems.

In automatic control engineering, there are several control architectures for mobile robotic systems. This is the case of intelligent control architectures in [14]–[18], optimal control architectures in [19]–[24], non-linear control architectures in [25]–[29]. However, in most robotic control systems, PWM drivers are unique interfacing techniques between feedback controllers and power electronic for robotic actuators. Therefore, the originality of this paper is to outline the feasibility of DCM drivers in a 2WD mobile robot, and to compare its performance to that of PWM drivers, under the same PID/LQRT-PSO controller, initiated in [30]. Without loss of generality, the development of kinematic and dynamic models (open or closed loop), and corresponding virtual simulation schemes, will be carried out on a prototyping 2WD mobile [30].

The next sections of the paper are organized as follow. Section 2 of this paper will focus on the methodology and tools for modeling of the 2WD mobile robot control system. Then, Dual architecture of mobile robot will be presented and discussed in Section 3. In section 4, global architecture with kinematic controller for tracking trajectory will be presented, results and discussion are presented in section 5. Finally, the paper will be concluded
in Section 6.

2. MODELING OF 2WD MOBILE ROBOT

Direct and inverse kinematic modeling

The kinematic model of the 2WD mobile robots is clearly stated and developed under certain assumptions in [30], its illustrative kinematic scheme is recalled in Figure 1 shows the corresponding kinematic model.

$$\begin{cases} \begin{cases} \dot{x}_a = v \cdot cos\theta \\ \dot{y}_a = v \cdot \sin\theta \end{cases} & (a) \\ v = \dfrac{v_g + v_d}{2} = R\dfrac{\omega_g + \omega_d}{2} & (b) \\ \omega = \dot{\theta} = R\dfrac{\omega_d - \omega_g}{2L} & (c) \end{cases} \tag{1}$$

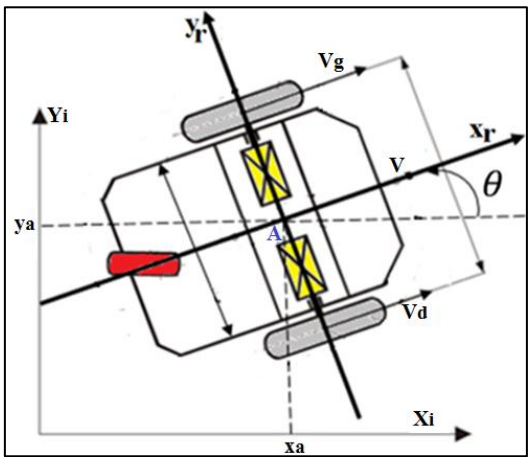

Fig. 1 2WD mobile robot 2D plane representation [30]

Furthermore, using equations (1.b) and (1.c), this leads to the inverse kinematic model translated by equations (2) and (3).

$$\omega_d = \frac{v + L\omega}{R} \tag{2}$$

$$\omega_g = \frac{v - L\omega}{R} \tag{3}$$

Where :

v – The linear speed ;

R – The radius of the wheel ;

ω – Angular velocity ;

L – Distance between the centreline and a wheel ;

v_g, ω_g – Left linear and angular velocity;

v_d, ω_d – Linear and right angular velocity;

Motors dynamic modeling

The dynamic model of servomotors associated with both wheels, was developed in [30] from experimental data, using Matlab system identification tool. It is described by equation (4). It should be noted that the two motors of the mobile robot are assumed to be identical and therefore have the same estimated transfer function model.

$$G_{OL}(s)=\frac{\Omega(s)}{U(s)}=\frac{41.83}{s^2+8.699s+12.91}$$
$$=\frac{K_s\ \omega_n^2}{s^2+2\ \xi\ \omega_n\ s+\omega_n^2} \quad (4)$$
$$K_s=\frac{41.83}{12.91},\ \omega_n=\sqrt{12.91},\ \ \xi=\frac{8.699}{2\ \omega_n}$$

Where, $G_{OL}(s)$ is open loop estimated transfer function of one motor, $\Omega(s)$ is the angular velocity and $U(s)$ the control voltage.

3. DUAL ARCHITECTURE OF 2WD MOBILE ROBOT

Analysis and modeling of Dual DCM Drivers

The implementation of the Dual Duty Cycle Modulator comes from the analysis of the single-channel analogue circuit based on passive components and an operational amplifier. However, as the number of servo mechanisms in the mobile robot is 2, this also implies two modulators. As shown in figure 2, a dual DCM, consists of 2 identical and independent circuits, each of which being a simple DCM driver.

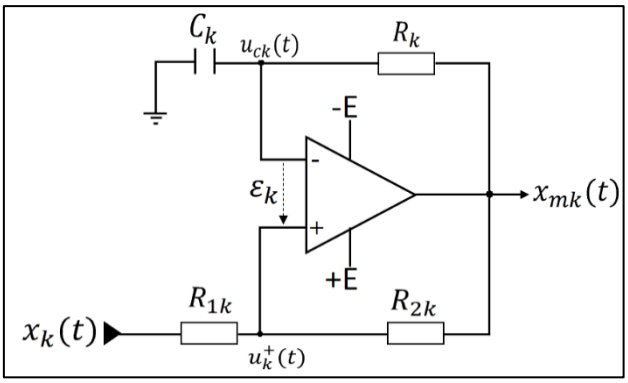

Fig. 2 Electronic circuit base of Dual DCM_k driver, k∈{1,2}

Figure 2 shows, among other things, the minimum number of passive and active components to be used. The analysis of the circuit allows us to establish the relations of the system of equations (5).

$$\begin{cases} u_k^+(t)=\dfrac{\dfrac{x_k(t)}{R_{1k}}+\dfrac{x_{mk}(t)}{R_{2k}}}{\dfrac{1}{R_{1k}}+\dfrac{1}{R_{2k}}}=\alpha_{1k}x_{mk}(t)+(1-\alpha_{1k})x_k(t) \quad (5.a) \\ \xi_k(t)=u_k^+(t)-u_{ck}(t) \qquad (5.b) \\ x_{mk}(t)=\begin{cases} E, & if\ \xi_k(t)\geq 0 \\ -E, & otherwise \end{cases} \qquad (5.c) \\ \dfrac{du_{ck}(t)}{dt}=-\dfrac{1}{\tau}u_{ck}(t)+\dfrac{1}{\tau}x_{mk}(t) \qquad (5.d) \end{cases} \quad (5)$$
$$with \quad \alpha_{1k}=\frac{R_{1k}}{R_{1k}+R_{2k}},\quad \tau=R_kC_k;\quad k\in\{1,2\}$$

A transformation of the dynamic equation (5.d) into the frequency domain leads to equation (6).

$$\frac{U_{ck}(s)}{X_{mk}(s)}=\frac{1}{1+\tau s} \quad (6)$$

From equations (5.a)-(5.c), and equation (6), one continuous model on Matlab/Simulink environment is illustrated in figure 3, for needs of conformity with the schematics of the servo structure for which they will be used as drivers.

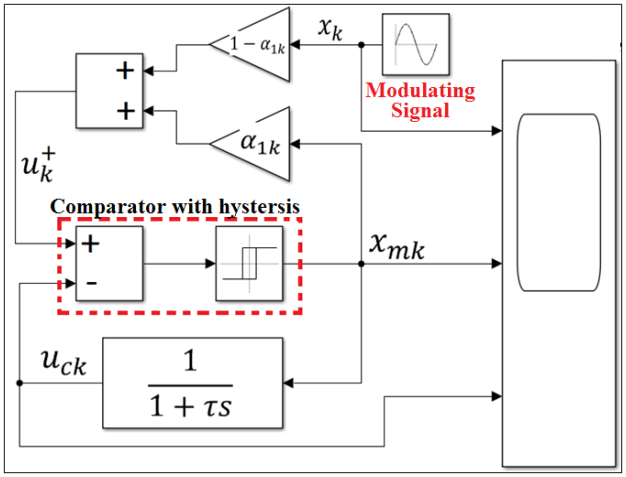

Fig. 3 Simulink DCM Driver Dual modeling scheme

Analysis and modeling of Dual PWM Drivers

Compared to DCM driver, the basic structure of the pulse width modulation (PWM) driver, show us, a high number of using active and passive components, as illustrated in figure 4. This basic modulator architecture structure is decomposable into three blocks, namely: block 1, representing a Schmitt trigger comparator, whose role is to generate square wave signals; block 2, representing an integrator, whose role is to transform the square wave signals from block 1 into a triangular signal; block 3, representing a simple comparator, whose role is to compare the signal from block 2 with the modulating signal, in order to produce a modulated signal x_k .

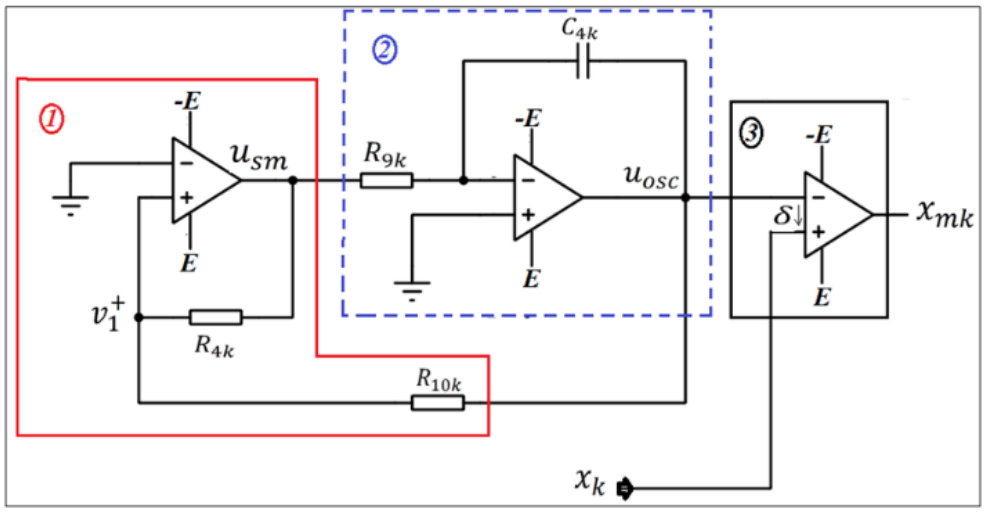

Fig. 4 Electronic circuit base of PWM_k driver, kϵ{1,2}

The analysis of the circuit in Figure 4 allows us to establish the system of equations (7).

$$\begin{cases} v_1^+(t) = \dfrac{\dfrac{u_{osc}(t)}{R_{10k}} + \dfrac{u_{sm}(t)}{R_{4k}}}{\dfrac{1}{R_{10k}} + \dfrac{1}{R_{4k}}} = \beta_{1k} u_{osc}(t) + (1-\beta_{1k}) u_{sm}(t) \quad (7.a) \\ \delta_k(t) = x_k(t) - u_{osc}(t) \quad (7.b) \\ x_{mk}(t) = \begin{cases} E, & if\ \delta_k(t) \geq 0 \\ -E, & otherwise \end{cases} \quad (7.c) \\ u_{osc}(t) = -\dfrac{1}{R_{9k}C_{4k}} \int u_{sm}(t)dt \quad (7.d) \end{cases} \tag{7}$$

$$with \quad \beta_{1k} = \frac{R_{4k}}{R_{4k} + R_{10k}}; \quad k \in \{1,2\}$$

$$with \quad \beta_{1k} = \frac{R_{4k}}{R_{4k} + R_{10k}}; \quad k \in \{1,2\}$$

A transformation of the dynamic equation (7.d) into the frequency domain leads to equation (8).

$$\frac{U_{osc}(s)}{U_{sm}(s)} = -\frac{1}{R_{9k}C_{4k}s} \tag{8}$$

From equations (7.a)-(7.c), and equation (8), one continuous model under the Matlab/Simulink environment is illustrated in figure 5.

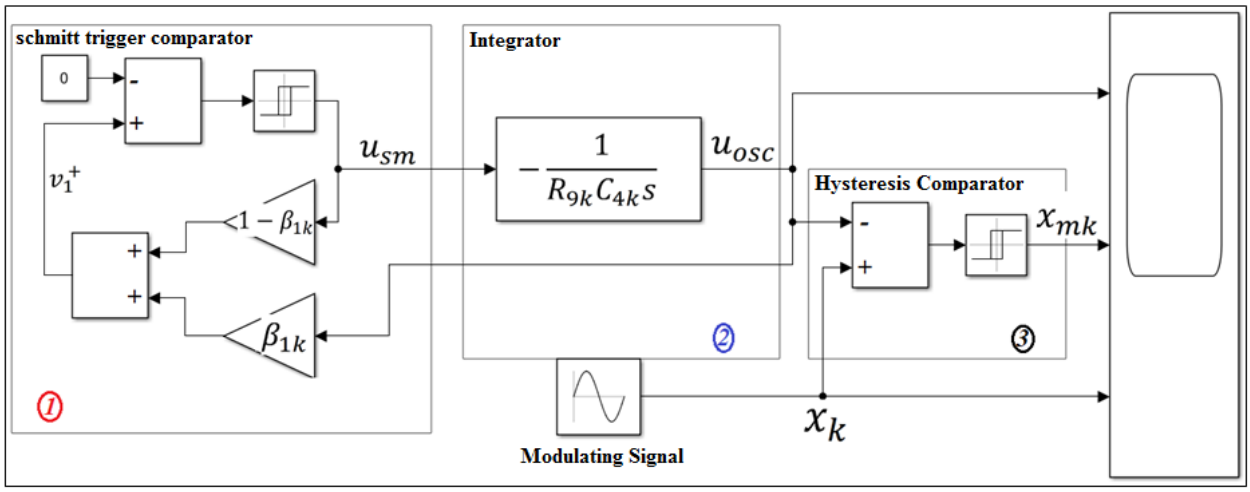

Fig. 5 Simulink PWM Driver Dual modeling scheme

Dual architecture of servomechanism feedback control with and without PWM/DCM Drivers
Channel open loop structure of servomechanism with and without PWM/DCM Drivers

A driver (PWM or DCM) such as illustrated in figures 3 and 5, should not modify the dynamic behavior of the power system to be controlled; this is why to evaluate this hypothesis, we must integrate it in an open chain in series with the system to be, controlled such as our servomechanisms. The Simulink model corresponding to the open loop representation with and without drivers is illustrated in figure 6.

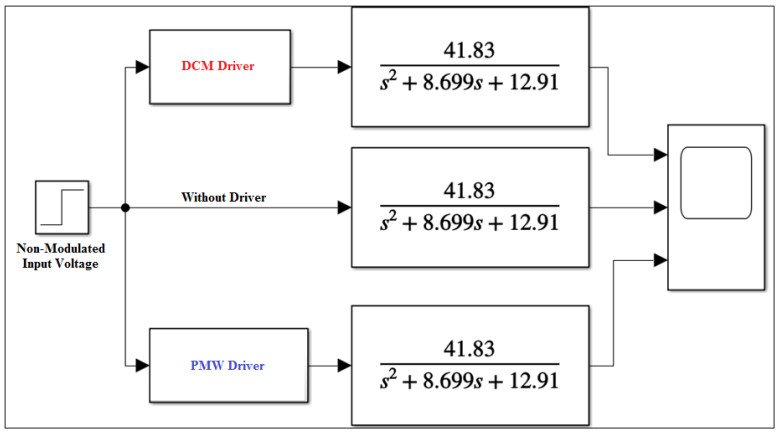

Fig. 6 Open Loop System of One Motor with and without Drivers DCM/PWM

1-Channel closed loop optimal structure PID/LQRT-PSO of servomechanism with and without PWM/DCM Drivers

The general structure of the classical servo system integrating the system parameters as illustrated in figure 7, represents the single-channel architecture without driver studied in the work of M. Mbihi et al [30]. At the output of the controller, our drivers will be integrated in order to evaluate the effects of the drivers on the servomechanism; as illustrated in Figure 8, the PID/LQRT-PSO controller will serve as a modulating signal for our different DCM and PWM drivers. A simulink block diagram representation of the single-channel servo is shown in Figure 8.

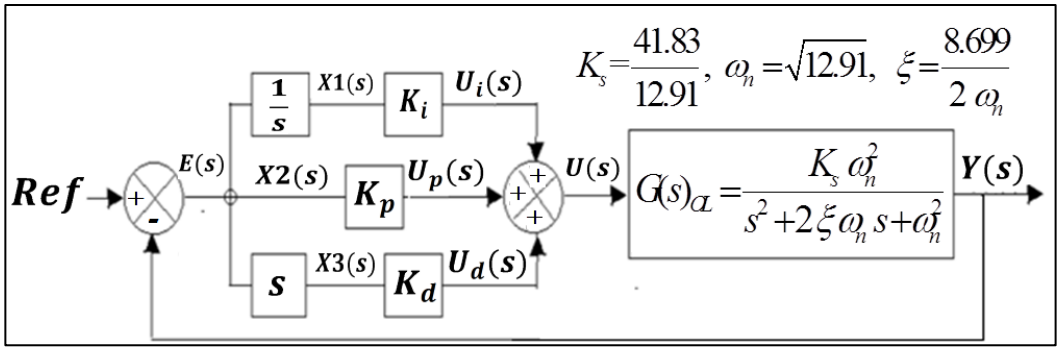

Fig. 7 Feedback control of one servomechanism of 2WD mobile robot [30]

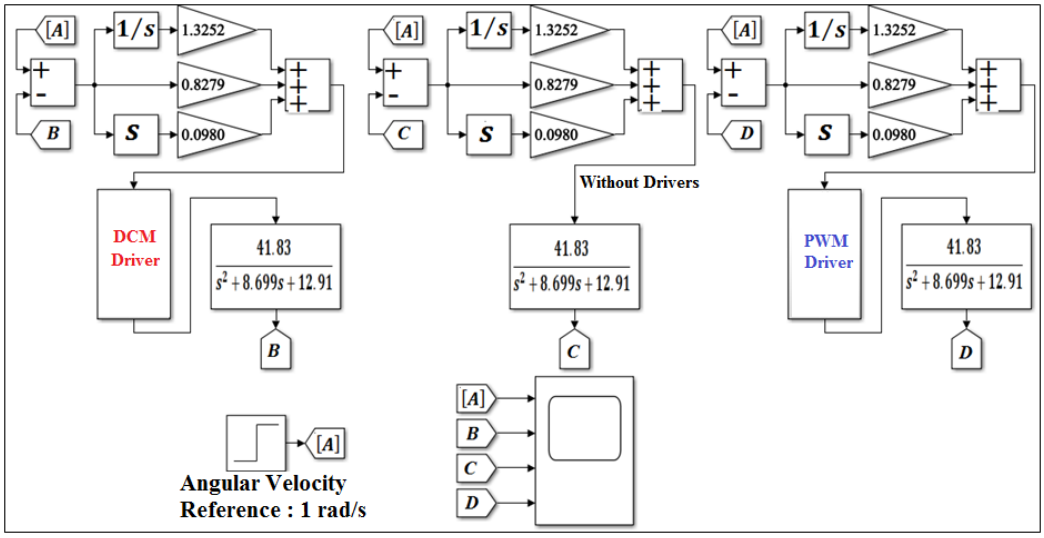

Fig. 8 PID/LQRT-PSO feedback control scheme of one servomechanism of 2WD mobile robot, with and without DCM/PWM Drivers

4. GLOBAL ARCHITECTURE WITH KINEMATIC CONTROLLER FOR TRAJECTORY FOLLOWING

Kinematic controller design

The kinematic controller designed on this paper is based on kinematic model of the 2WD mobile robot, given in equation (1). This approach is also used in [31]. For good practice, equation (1) can be re-written considering the small distance between gravity center of the mobile robot and the center from traction wheels axis:

$$\begin{bmatrix} \dot{x} \\ \dot{y} \\ \dot{\theta} \end{bmatrix} = \begin{bmatrix} \cos\theta & -a\sin\theta \\ \sin\theta & a\cos\theta \\ 0 & 1 \end{bmatrix} \begin{bmatrix} v \\ \omega \end{bmatrix} = M.h^c \tag{9}$$

With,

$$M = \begin{bmatrix} \cos\theta & -a\sin\theta \\ \sin\theta & a\cos\theta \\ 0 & 1 \end{bmatrix} \quad and \quad h^c = \begin{bmatrix} v \\ \omega \end{bmatrix}$$

Where in the M matrix:
a: is the distance between gravity center of the mobile robot and the center from traction wheels axis.

The new inverse kinematic can be obtained:

$$h^c = M_{INV} \begin{bmatrix} \dot{x} \\ \dot{y} \end{bmatrix} = \left(M\left(1:2,:\right) \right)^{-1} \begin{bmatrix} \dot{x} \\ \dot{y} \end{bmatrix} \tag{10}$$

$$with \quad M_{INV} = \begin{bmatrix} \cos\theta & \sin\theta \\ -\frac{1}{a}\sin\theta & \frac{1}{a}\cos\theta \end{bmatrix}$$

Therefore, F. Martins in [31] proved that, to obtain references velocities (linear and angular) and also have the kinematic controller based on kinematic inverse, using equation (11) :

$$h_{ref}^c = M^{-1} \begin{bmatrix} \dot{x}_{ref} + \zeta_x \tanh\left(\frac{k_x}{\zeta_x}\left(x_{ref} - x \right) \right) \\ \dot{y}_{ref} + \zeta_y \tanh\left(\frac{k_y}{\zeta_y}\left(y_{ref} - y \right) \right) \end{bmatrix} \tag{11}$$

With $h_{ref}^c = \begin{bmatrix} v_{ref} \\ \omega_{ref} \end{bmatrix}$;

x_{ref} , x are respectively the desired position and current position on X-axis; y_{ref} , y respectively the desired position and current position on Y-axis; ζ_x, ζ_y are real saturation constants; k_x, k_y are gains of controller strictly positive.

Stability analysis

In this analysis, some assumptions are considered such as perfect equality references velocities. So, the expression that illustrate the previous assumption is given by:

$$h^c = h_{ref}^c \tag{12}$$

Which can also be rewritten as:

$$\begin{bmatrix} \dot{x} \\ \dot{y} \end{bmatrix} = \begin{bmatrix} \dot{x}_{ref} + \zeta_x \tanh\left(\frac{k_x}{\zeta_x}\left(x_{ref} - x\right)\right) \\ \dot{y}_{ref} + \zeta_y \tanh\left(\frac{k_y}{\zeta_y}\left(y_{ref} - y\right)\right) \end{bmatrix} \tag{13}$$

And we have:

$$\begin{bmatrix} \dot{x}_{ref} - \dot{x} \\ \dot{y}_{ref} - \dot{y} \end{bmatrix} + \begin{bmatrix} \zeta_x \tanh\left(\frac{k_x}{\zeta_x}\left(x_{ref} - x\right)\right) \\ \zeta_y \tanh\left(\frac{k_y}{\zeta_y}\left(y_{ref} - y\right)\right) \end{bmatrix} = \begin{bmatrix} 0 \\ 0 \end{bmatrix} \tag{14}$$

Let $\dot{x}_{err} = \dot{x}_{ref} - \dot{x}$ and let $\dot{y}_{err} = \dot{y}_{ref} - \dot{y}$, equation (14) becomes:

$$\begin{bmatrix} \dot{x}_{err} \\ \dot{y}_{err} \end{bmatrix} + \begin{bmatrix} \zeta_x \tanh\left(\frac{k_x}{\zeta_x}\left(x_{ref} - x\right)\right) \\ \zeta_y \tanh\left(\frac{k_y}{\zeta_y}\left(y_{ref} - y\right)\right) \end{bmatrix} = \begin{bmatrix} 0 \\ 0 \end{bmatrix} \tag{15}$$

Equation (15) has a unique equilibrium point at the origin. Considering:

$$\dot{\wp} = -\begin{bmatrix} \dot{x}_{err} \\ \dot{y}_{err} \end{bmatrix} = -\begin{bmatrix} \zeta_x \tanh\left(\frac{k_x}{\zeta_x}\left(x_{ref} - x\right)\right) \\ \zeta_y \tanh\left(\frac{k_y}{\zeta_y}\left(y_{ref} - y\right)\right) \end{bmatrix} \tag{16}$$

Where $\wp^T = \begin{bmatrix} x_{err} & y_{err} \end{bmatrix}^T$ is the output error vector.

Then, to analyse the stability looking Lyapunov, it's necessary to choose the appropriate candidate function given in equation (17):

$$V = \frac{1}{2}\wp^T\wp \tag{17}$$

Where V is the Lyapunov candidate function, positive definite. The derivative of the Lyapunov candidate function is given as follow:

$$\dot{V} = \wp^T\dot{\wp} = -x_{err}\zeta_x \tanh\left(\frac{k_x}{\zeta_x}x_{err}\right) - y_{err}\zeta_y \tanh\left(\frac{k_y}{\zeta_y}y_{err}\right) \tag{18}$$

With $x_{err} = x_{ref} - x \quad and \quad y_{err} = y_{ref} - y$

Equation (18) is strictly negative, then the proposed kinematic controller is considered asymptotically stable around equilibrium point at origin.

Architecture of global 2WD mobile robot with kinematic controller

In this architecture, only dual DCM Driver structure is considered and adding of kinematic control from good tracking trajectory as illustrated in Figure 9. We can notice that, in the multiple trajectories block, illustrated in this figure, the input named Trajectory is connected to a constant taking 4 different numerical values $\{1, 2, 3 \; or \; 4\}$ and symbolising the different types of reference trajectories.

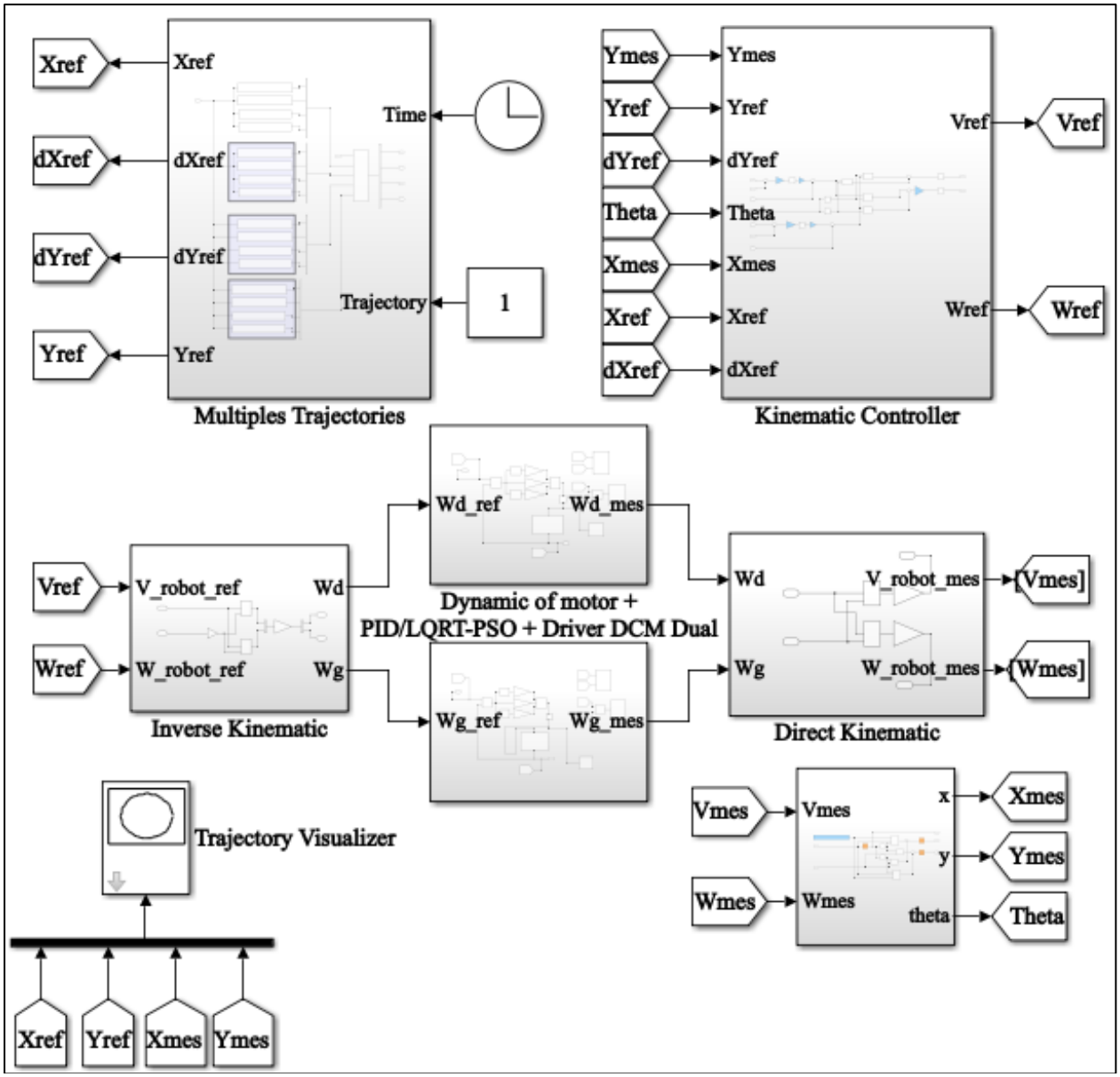

Fig. 9 Global Simulink architecture of 2WD mobile robot including kinematic controller

5. RESULTS AND DISCUSSION

Simulation result of PWM/DCM driver

We present the simulation results for Figures 3 and 5 to show that our Simulink driver models do indeed respond while observing the behaviour of our modulated signals. We use as modulant, a sine wave from a signal generator parameterized for a maximum amplitude of 2 Volts with the signal frequency equal to 5 kHz. The simulation parameters are shown in Table 1.

Table-1 Simulation parameters of PWM and DCM Drivers

N°		Parameters	Values
1	**PWM_k** Circuit	R_{4k}	10 $k\Omega$
		R_{9k}	1.4667 $k\Omega$
		R_{10k}	1.7206 $k\Omega$

		C_{4k}	33 nF
		E	± 9 V
		f_m^{PWM}	30 kHz
2	DCM_k Circuit	R_k	2.320 $k\Omega$
		C_k	33 nF
		R_{1k}	2 $k\Omega$
		R_{2k}	16.6742 $k\Omega$
		E	± 9 V
		$f_m^{DCM}(0)$	30.372 kHz
3	Sine Signal Generator	A_m	2 V
		f_s	5 kHz

The simulation results are shown in Figures 10 and 11 for the PWMk circuit and the DCMk circuit respectively.

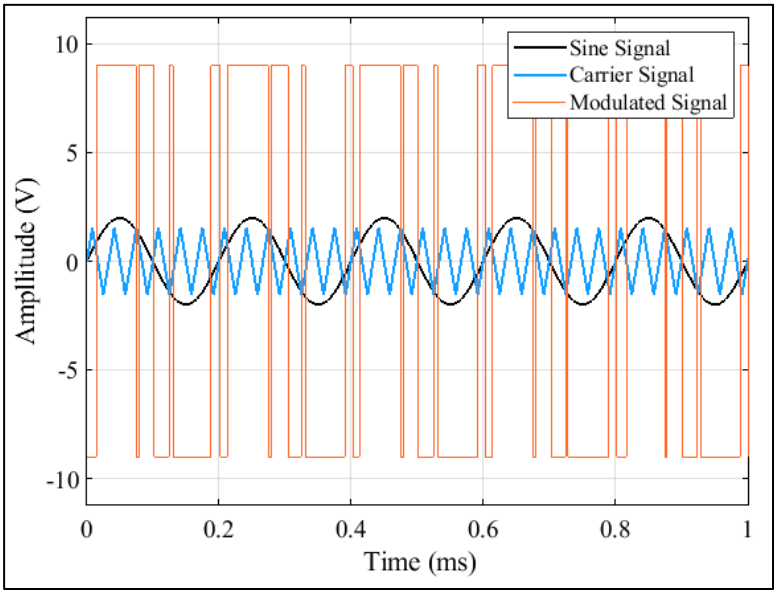

Fig. 10 Sine signal modulated by PWM circuit

The curve shown in black in Figure 10 represents our modulating signal and describes a sine wave with the amplitude and frequency given in Table 1. The sawtooth signal, also known as the carrier, is generated by a triangular oscillator, which is compared by means of an operational amplifier materialized in Simulink by hysteresis threshold comparator in order to obtain a modulated signal illustrated in blue with constant modulation frequency.

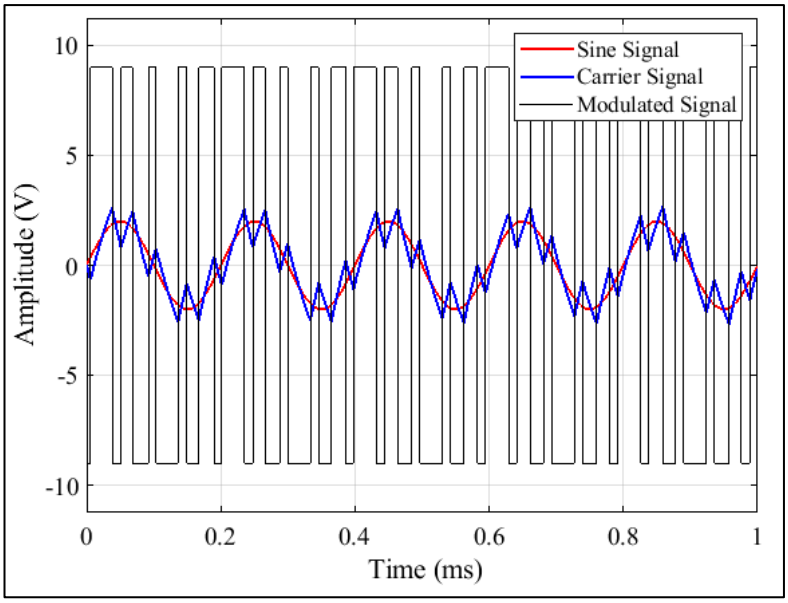

Fig. 11 Sine signal modulated by DCM circuit

The curve observed in red in figure 11 represents our modulating signal and describes a sine wave with the amplitude and frequency indicated in Table 1. The sawtooth signal, also known as the carrier, is generated by charging and discharging a capacitor which represents our oscillator; we note that the carrier has a tracking effect on the modulating signal; we thus have a modulated signal in black with variable frequency, and function of the modulating signal.

Open loop simulation result of motor control

Figure 12 shows the open-loop simulation of a 2WD mobile robot motor to which an input voltage of 1Volt is applied; the simulation block diagram is shown in Figure 6. Based on the assumption that a good driver should not influence the dynamic behaviour of a system in any way, we can see from the simulation results presented that the angular velocity of the motor with the DCM base driver behaves identically to that without the driver; this is not the case with the PWM base driver; this is illustrated in figure 13 by the angular velocity error curve materialising the fidelity of the dynamic behaviour of the experimentally modelled motor when a control voltage is applied across its terminals with and without DCM driver.

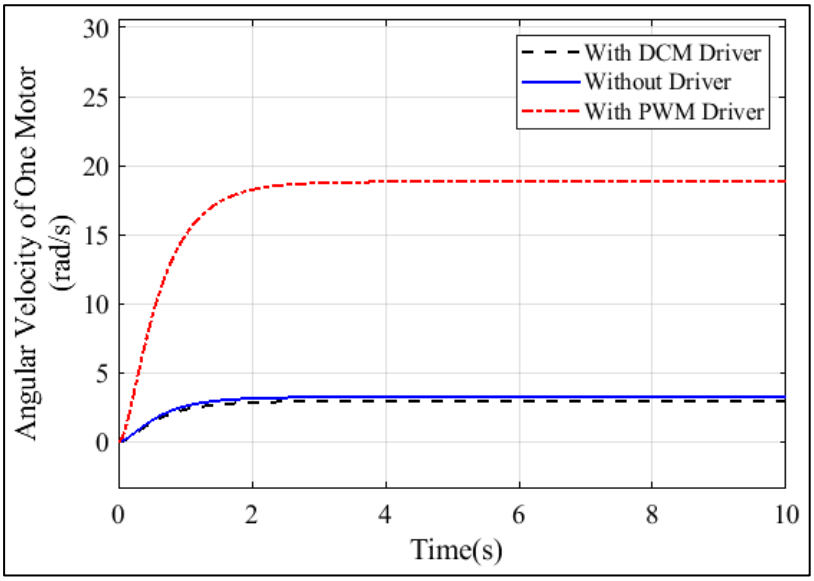

Fig. 11 Open loop simulation of angular velocity of one motor controlled with and without PWM/DCM Drivers

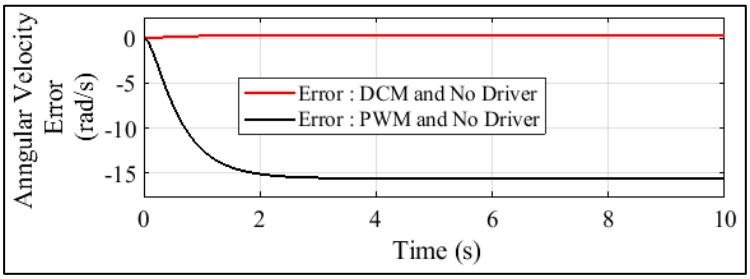

Fig. 12 Angular velocity error with PWM/DCM Driver and No Driver

Closed loop simulation result with 1-Channel Driver PWM/DCM

The block diagram illustrated in figure 8, allows us to obtain the simulation results of the single-channel servo control of the angular velocity of a motor with and without driver, illustrated in figure 14. We can see that the dynamic behaviour of the motor when driven by a basic DCM driver is identical to that of the motor when it is without a driver. On the other hand, with a basic PWM driver, we have a different dynamic behaviour in the transient regime. This allows us to affirm that the modelled duty cycle modulator satisfies the requirements of a good driver in terms of energy transfer without significant impact on of the dynamic behaviour of the kinematic system to be driven.

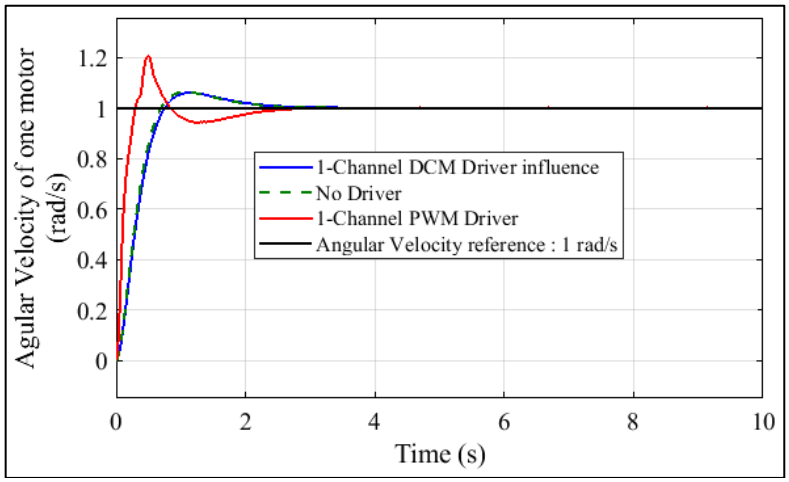

Fig. 13 Closed loop simulation of angular velocity of one motor controlled with and without PWM/DCM Drivers

Global simulation results of tracking trajectory

In this sub-section, simulation of global system in figure 9, of 2WD mobile robot is illustrated. Parameters simulations is illustrated in Table 2.

Table-2 Simulation parameters

Kinematics parameters controllers	*Values (without unit)*
k_x	14.0
k_y	7.0
ζ_x	0.85
ζ_y	0.85
2WD mobile robot kinematics parameters	Values (m)
L	0.0675
R	0.0163
a	0.045

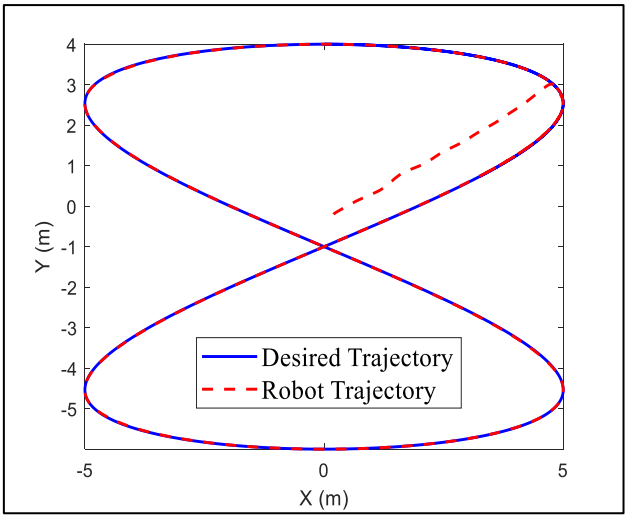

Fig. 14 8-shape trajectory

The figure 15, illustrated 8-shape trajectory tracked by the 2WD mobile robot. Figure 16 and 18 illustrated linear X-axis and linear Y-axis position of mobile robot.

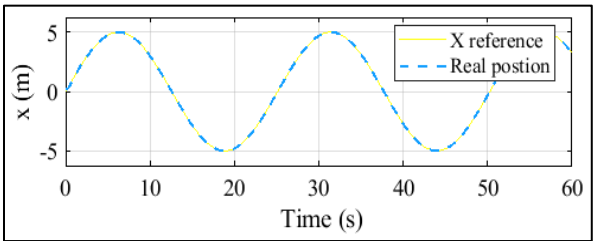

Fig. 15 X Reference and Real Position

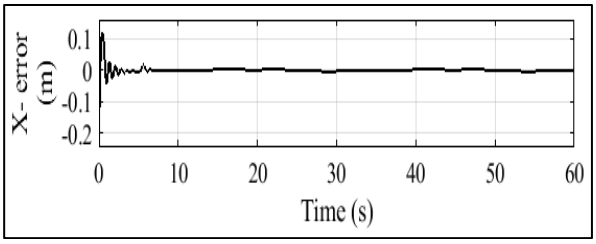

Fig. 16 Error X Position

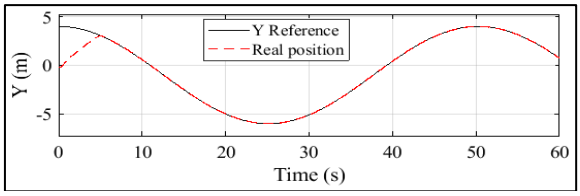

Fig. 17 Y Reference and Real Position

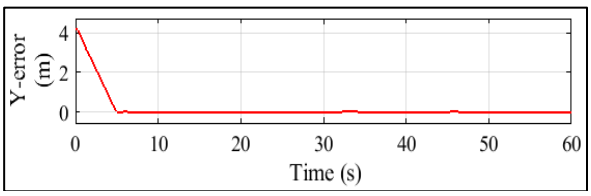

Fig. 18 Error Y Position

Figures 17 and 19 illustrates the X error and Y error respectively when the mobile robot track the trajectory. The figures 20 and 22 outline comparison between the reference of linear and angular velocities and their measurements respectively. Figures 21 and 23 show error linear and error angular velocities.

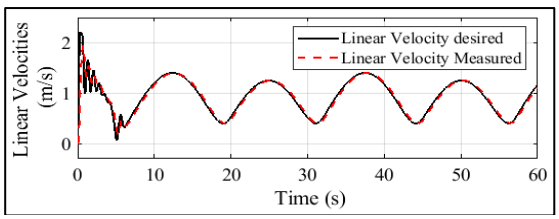

Fig. 19 Linear velocity of mobile robot

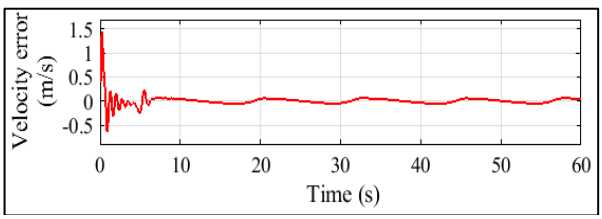

Fig. 20 Error Linear velocity

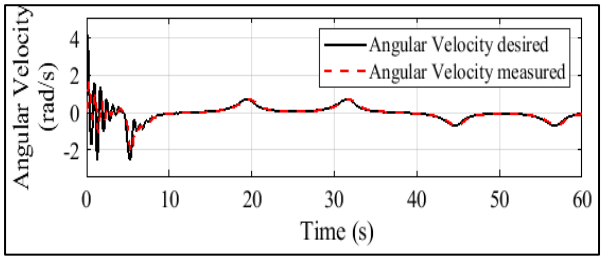

Fig. 21 Angular velocity of mobile robot

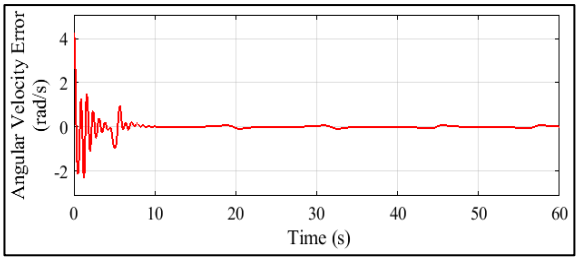

Fig. 22 Error Angular velocity

Furthermore, mobile robot moves using more energy control that the left and right energy control are illustrated respectively in Figure 24 and 25.

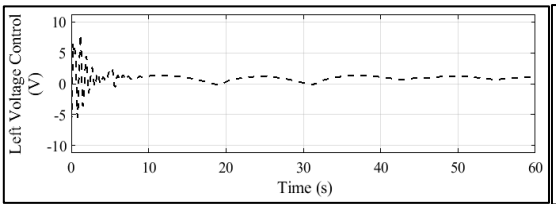

Fig. 23 Left voltage Control

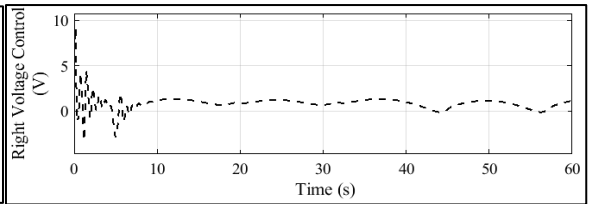

Fig. 24 Right voltage Control

Others trajectories, as illustrated in figures 26 and 27, are simulated for showing stability of the kinematic controller.

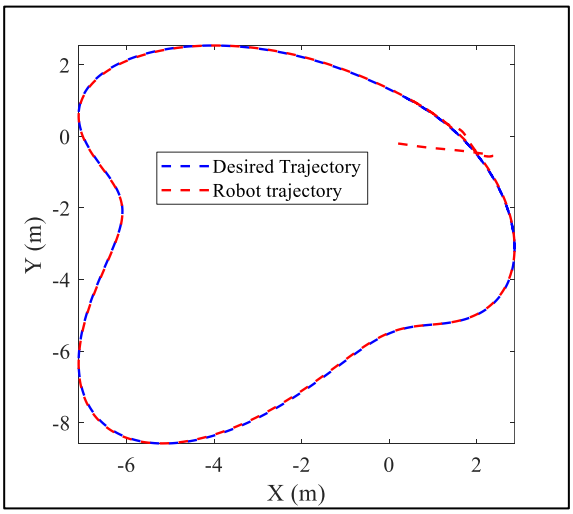

Fig. 25 Deformed circle Trajectory

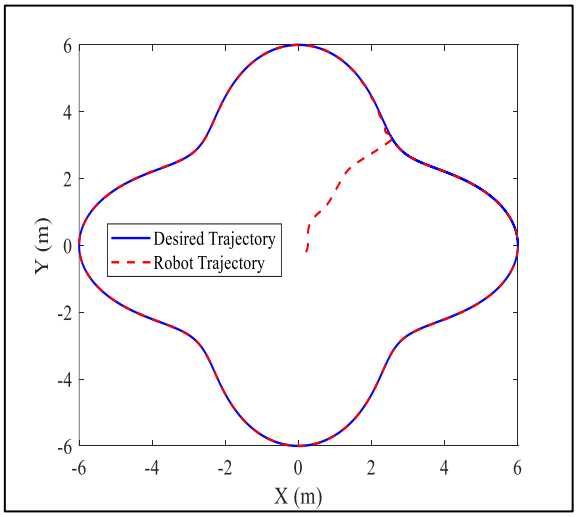

Fig. 26 Flower Trajectory

6. CONCLUSION

The feasibility study and performance analysis of dual DCM drivers for 2WD mobile robots in trajectory tracking applications, have been relevant motivating factors of the research work presented in this paper. Following the state of the art on DCM and PWM applications, we significantly contributed to new analytical developments and virtual simulation models of Dual DCM drivers in Matlab/Simulink framework, with successful applications to trajectory tracking systems for mobile robots. The PID/LQRT-PSO control law through DCM driver used have any disturbance and allow the mobile to track with precision different trajectory. However, parameters of kinematic controller are chosen by trial and error. Therefore, in a future work, it's important to determine theses parameters of kinematic controller by an optimization algorithm like

particle swarm optimization. Furthermore, it would be a significant contribution to validate the high safetyness, quality and performance in the experimental test involving a real prototyping 2WD mobile robot.

APPENDIX

Notice that some equations are necessary to compute PWM and DCM frequency values. Then, the PWM modulating frequency f_m^{PWM} is computed by:

$$f_m^{PWM} = \frac{R_{4k}}{4R_{10k}\ R_{9k}\ C_k}$$

And DCM modulating frequency $f_m^{DCM}\left(x_{mk}\right)$ is computed considering the modulating signal $x_{mk}\left(t\right)$.

$$f_m^{DCM}\left(x_{mk}\right) = \frac{1}{\tau \log\left(\frac{\left(\alpha_{2k}x_{mk}\right)^2 - \left(\left(1+\alpha_{1k}\right)E\right)^2}{\left(\alpha_{2k}x_{mk}\right)^2 - \left(\left(\alpha_{1k}-1\right)E\right)^2}\right)}$$

Considering $x_{mk}\left(t\right) = 0,$ we have the basic DCM modulating frequency $f_m^{DCM}\left(0\right).$

$$f_m^{DCM}\left(0\right) = \frac{1}{\tau \log\left(\frac{\left(\left(1+\alpha_{1k}\right)E\right)^2}{\left(\left(\alpha_{1k}-1\right)E\right)^2}\right)}$$

REFERENCES

[1] J. Mbihi, B. Ndjali, and M. Mbouenda, "Modelling and Simulation of a Class of Duty-Cycle Modulators for Industrial Instrumentation," *Iran. J. Electr. Comput. Eng.*, vol. 4, no. 2, pp. 121–128, 2005.

[2] J. Mbihi, F. N. Beng, M. Kom, and L. N. Nneme, "A Novel Analog-to-Digital Conversion Technique Using Nonlinear Duty-Cycle Modulation," *Int. J. Electron. Comput. Sci. Eng.*, vol. 1, no. 3, pp. 818–825, 2012.

[3] G. B. Sonfack and J. Mbihi, "FPGA-Based Analog-to-Digital Conversion via Optimal Duty-Cycle Modulation," *Electr. Electron. Eng.*, vol. 8, no. 2, pp. 29–36, 2018, doi: 10.5923/j.eee.20180802.01.

[4] G. Sonfack, J. Mbihi, and B. Moffo Lonla, "Optimal Duty-Cycle Modulation Scheme for Analog-To-Digital Conversion Systems," *World Acad. Sci. Eng. Technol. Int. J. Electonics Commun. Eng.*, vol. 11, no. 3, pp. 354–360, 2017.

[5] J. Mbihi and L. N. Nneme, "A Multi-Channel Analog-To-Digital Conversion Technique Using Parallel Duty-Cycle Modulation," *Int. J. Electron. Comput. Sci. Eng.*, vol. 1, no. 3, pp. 826–833, 2012.

[6] B. L. Moffo and J. Mbihi, "A Novel Digital Duty-Cycle Modulation Scheme for FPGA-Based Digital-to-Analog Conversion," *IEEE Trans. CIRCUITS Syst.*, vol. 62, no. 6, pp. 543–547, 2015.

[7] O. S. Ulriche, M. L. Bertrand, G. N. E. R. Christian, and M. Jean, "A novel FPGA-Based Multi-Channel Signal Acquisition System Using Parallel Duty-Cycle Modulation and Application to Biologic Signals : Design and Simulation," *J. Electr. Eng. Electron. Control Comput. Sci. – JEEECCS*, vol. 7, no. 24, pp. 13–20, 2021.

[8] L. N. Nneme and J. Mbihi, "Modeling and Simulation of a New Duty-Cycle Modulation Scheme for Signal Transmission Systems," *Am. J. Electr. Electron. Eng.*, vol. 2, no. 3, pp. 82–87, 2014, doi: 10.12691/ajeee-2-3-4.

[9] Y. Paulin, D. Sounsoumou, J. Mbihi, and Y. Effa, "Modélisation et simulation virtuelle d ' un nouveau schéma de réglage de hacheurs Boost à commande rapprochée par modulation en rapport cyclique Résumé," *Afrique Sci.*, vol. 13, no. 1, pp. 176–185, 2017.

[10] D. Sounsoumou, Y. Paulin, M. Jean, H. Djalo, and E. Joseph, "Virtual Digital Control Scheme for a Duty-Cycle Modulation Boost Converter," *J. Comput. Sci. Control Syst.*, vol. 10, no. 2, pp. 22–27, 2017.

[11] P. O. Etouke, L. N. Nneme, and J. Mbihi, "An Optimal Control Scheme for a Class of Duty-Cycle Modulation Buck Choppers : Analog Design and Virtual Simulation," *J. Electr. Eng. Electron. Control Comput. Sci. – JEEECCS*, vol. 6, no. 19, pp. 13–20, 2020.

[12] A. O. Biyobo and J. Mbihi, "A Novel Sine Duty-Cycle Modulation Control Scheme for Photovoltaic Single-Phase Power Inverters Research Laboratory of Computer Science Engineering and Automation Research Laboratory of Computer Science Engineering and Automation," *WSEAS Trans. CIRCUITS Syst.*, vol. 17, pp. 105–113, 2018.

[13] A. O. Biyobo *et al.*, "Étude expérimentale d'un nouveau modèle d'onduleur solaire monophasé à modulation en rapport cyclique," *Afrique Sci.*, vol. 16, no. 2, pp. 118–131, 2020.

[14] M. Khodja and S. Mahfoudhi, "The Use of an Optimal Fuzzy Controller Algorithm for a Low-cost Microcontroller," *Int. J. Intell. Eng. Syst.*, vol. 14, no. 5, pp. 283–293, 2021, doi: 10.22266/ijies2021.1031.26.

[15] J. Blaise, M. Zanga, and B. M. Lonla, "Fuzzy-FOPIDF control for tracking the trajectory of nonholonomic Wheeled Mobile Robot," *J. Electr. Eng. Electron. Control Comput. Sci. – JEEECCS*, vol. 8, no. 28, pp. 29–38, 2022.

[16] M. M. Joshi and M. A. Zaveri, "Neuro-fuzzy based autonomous mobile robot navigation system," in *11th International Conference on Control, Automation, Robotics and Vision, ICARCV 2010*, 2010, pp. 384–389. doi: 10.1109/ICARCV.2010.5707354.

[17] L. A. Yekinni and A. Dan-Isa, "Fuzzy Logic Control of Goal-Seeking 2-Wheel Differential Mobile Robot Using Unicycle Approach," in *2019 IEEE International Conference on Automatic Control and Intelligent Systems, I2CACIS 2019 - Proceedings*, 2019, no. June, pp. 300–304. doi: 10.1109/I2CACIS.2019.8825082.

[18] M. Białek, P. Nowak, and D. Rybarczyk, "Application of an artificial neural network for planning the trajectory of a mobile robot," *J. Autom. Mob. Robot. Intell. Syst.*, vol. 14, no. 1, pp. 13–23, 2020, doi: 10.14313/JAMRIS/1-2020/2.

[19] E. Faculty, "Modeling and Optimal Trajectory Tracking Control of Wheeled a Mobile Robot," *Cauc. J. Sci.*, vol. 6, no. 2, pp. 137–146, 2019.

[20] T. Abut, M. Hüseyinoğlu, and A. Makalesi, "Modeling and Optimal Trajectory Tracking Control of Wheeled a Mobile Robot," *Cauc. J. Sci.*, vol. 6, no. 2, pp. 2148–6840, 2019, [Online]. Available: www.cjoscience.com

[21] A. Abbasi and A. J. Moshayedi, "Trajectory tracking of two-wheeled mobile robots, using LQR optimal control method, based on computational model of KHEPERA IV," *J. Simul. Anal. Nov. Technol. Mech. Eng.*, vol. 10, no. 3, pp. 41–50, 2018.

[22] A. J. Moshayedi, "Trajectory Tracking of Two-Wheeled Mobile Robots , Using LQR Optimal Control Method , Based On Computational Model of KHEPERA IV," *J. Simul. Anal. Nov. Technol. Mech. Eng.*, vol. 3, no. 10, pp. 0041–0050, 2017.

[23] J. B. He, Q. G. Wang, and T. H. Lee, "PI/PID controller tuning via LQR approach," in *Proceedings of the IEEE Conference on Decision and Control*, 1998, vol. 1, no. December, pp. 1177–1182. doi: 10.1109/cdc.1998.760858.

[24] J. B. He, Q. G. Wang, and T. H. Lee, "PI/PID controller tuning via LQR approach," *Chem. Eng. Sci.*, vol. 55, no. 13, pp. 2429–2439, 2000, doi: 10.1016/S0009-2509(99)00512-6.

[25] N. H. Hadi and K. K. Younus, "Path tracking and backstepping control for a wheeled mobile robot (WMR) in a slipping environment," *IOP Conf. Ser. Mater. Sci. Eng.*, vol. 671, no. 1, 2020, doi: 10.1088/1757-899X/671/1/012005.

[26] M. KALYONCU and F. DEMİRBAŞ, "Differential Drive Mobile Robot Trajectory Tracking With Using Pid and Kinematic Based Backstepping Controller," *Selcuk Univ. J. Eng. ,Science Technol.*, vol. 5, no. 1, pp. 1–15, 2017, doi: 10.15317/scitech.2017.65.

[27] X. Wu, P. Jin, T. Zou, Z. Qi, H. Xiao, and P. Lou, "Backstepping Trajectory Tracking Based on Fuzzy Sliding Mode Control for Differential Mobile Robots," *J. Intell. Robot. Syst. Theory Appl.*, vol. 96, no. 1, pp. 109–121, 2019, doi: 10.1007/s10846-019-00980-9.

[28] B. Ibari *et al.*, "Backstepping Approach for Autonomous Mobile Robot Trajectory Tracking," *Indones. J. Electr. Eng. Comput. Sci. IAES*, vol. 2, no. 3, pp. 478–485, 2016, doi: 10.11591/ijeecs.v2.i3.pp478-485 . hal-01328410 HAL.

[29] M. Hosein and A. Mohammadion, "Trajectory Tracking Weeled Mobile Robot Using Backstepping Method with Connection off Axle Trailer," *Int. J. Smart Electr. Eng.*, vol. 7, no. 4, pp. 177–187, 2018.

[30] M. D. Mbihi, B. L. Moffo, and L. N. Nneme, "Design and Virtual Simulation of an Optimal PID / LQRT-PSO ControlSystem for 2WD Mobile Robots," *Alger. J. signals Syst.*, vol. 6, no. 2, pp. 98–111, 2021.

[31] F. N. Martins, W. C. Celeste, R. Carelli, M. Sarcinelli-Filho, and T. F. Bastos-Filho, "An adaptive dynamic controller for autonomous mobile robot trajectory tracking," *Control Eng. Pract.*, vol. 16, no.

11, pp. 1354–1363, 2008, doi: 10.1016/j.conengprac.2008.03.004.